IMPACT OF ECCENTRICITY ON EAST-WEST STATIONKEEPING FOR THE GPS CLASS OF ORBITS

Todd A. Ely*

A strong relationship exists between eccentricity and the potential for an orbit with a mean motion commensurability to the Earth's rotation rate to be chaotic. These complex motions can significantly impact the east-west stationkeeping process for maintaining the repeating groundtrack property of a commensurate orbit. The focus of the current study is to investigate orbits with characteristics that are similar to GPS satellites except with modestly larger eccentricities. It will be shown that at eccentricities larger than ~ .01 the chaotic regions become significant, and the need arises for a robust stable stationkeeping approach. Furthermore, the investigation will develop an analytical model for eccentricity and show the factors that contribute to its growth, thus increasing the probability of encountering chaotic motion during a typical satellite lifetime. These results are applied to selected GPS orbits. It is determined that if the initial eccentricity is sufficiently large, then the traditional SK methods can destabilize and a more robust technique is required.

INTRODUCTION

A strong relationship exists between eccentricity and the potential for an orbit with a mean motion commensurability to the Earth's rotation rate (i.e., repeating groundtrack orbits) to be chaotic.[1] This is true at all values of eccentricity, but, perhaps most dramatic, is that it is true even for orbits that are nearly circular. These complex motions can have a significant impact on the east-west stationkeeping process that maintains a commensurate orbit's repeating groundtrack property. Ely and Howell[2] have shown that traditional stationkeeping (SK) methods are unable to maintain a repeating groundtrack in the presence of complex dynamics, such as with chaotic motion. They developed an alternate SK method, called eccentric orbit stationkeeping (EOSK), that has proven successful at maintaing a repeating groundtrack for eccentric, commensurate orbits. In particular, eccentric orbits are more likely to encounter stroboscopic nodal accelerations (or an equivalent action rate) that pass through a value of zero and destabilize the traditional SK methods. The EOSK approach has demonstrated its ability to remain convergent in the presence of these zeros.

The focus of the current study is to investigate satellite orbits with characteristics that are similar to those used by the Global Positioning System (GPS) except the eccentricities used are modestly larger. It will be shown that at eccentricities larger than ~ .01 the chaotic regions become significant, and the need arises for a robust stationkeeping

* Staff Engineer, Navigation and Flight Mechanics Section, Jet Propulsion Laboratory, California Institute of Technology, Pasadena, CA 91109.

approach, such as the EOSK approach. Furthermore, the investigation reveals that the influence of luni-solar perturbations and tesseral perturbations (with a stationary stroboscopic node) contribute to the growth of eccentricity, and, thus, increases the probability of encountering nodal accelerations that pass through a zero. Selected GPS orbits are examined and found, given certain conditions on initial values, to need the EOSK algorithm to maintain track.

FORMAL MODEL DEFINITION

A general long period dynamical model for the orbits considered in this study can be represented formally as an integrable Hamiltonian $H_o(I)$ being perturbed by additional conservative terms $\varepsilon H_1(I,\theta)$. The following is a brief summary of the relevant perturbations, a detailed development of the model can be found in reference [3]. The Hamiltonian is transformed into a set of action/angle variables (I,θ) that prove convenient for studying mean motion resonances with the Earth.[1] Included in H_o is the inverse square gravity term from a spherical Earth, a secular term due to the Earth's oblateness (i.e., the potential energy term V^{OB}), and an additional term introduced because the reference frame is fixed in the Earth and rotates with it. The perturbation $\varepsilon H_1(I,\theta)$ includes long period potential energy terms from the Earth's tesseral harmonics (longitude dependent) $V^{\mathcal{T}}$, the Earth's zonal harmonics (longitude independent) $V^{\mathcal{Z}}$, the Moon's harmonics $V^{\mathcal{L}}$, and the Sun's harmonics $V^{\mathcal{S}}$. Note, the superscript $\mathcal{OB}$ is used when referring to Earth oblateness, $\mathcal{T}$ for tesseral terms, $\mathcal{Z}$ for zonal terms, $\mathcal{L}$ for lunar quantities, and $\mathcal{S}$ for solar quantities. Formally, the Hamiltonian takes the following form,

$$H = H_o(I) + \varepsilon H_1(I,\theta), \tag{1}$$

$$\begin{aligned} H = -\frac{s_o^2\mu^2}{2I_1^2} - \dot{\theta}_e I_1 + V^{OB}(I_1,I_2,I_3) + \sum V^{\mathcal{T}}(I_1,I_2,I_3,\lambda,\omega) + \sum V^{\mathcal{Z}}(I_1,I_2,I_3,\omega) + \\ \sum V^{\mathcal{L}}(I_1,I_2,I_3,\omega,\Omega,\Omega_{\mathcal{L}}) + \sum V^{\mathcal{S}}(I_1,I_2,I_3,\omega,\Omega,\Omega_{\mathcal{S}}), \end{aligned} \tag{2}$$

where the action/angle pairs are defined as follows,

$$\begin{aligned} I_1 &= s_o L = s_o\sqrt{\mu a}, & \lambda &= \frac{1}{s_o}(M+\omega) - (\theta_e - \Omega); \\ I_2 &= L\sqrt{1-e^2} - L, & \omega; \\ I_3 &= L\sqrt{1-e^2}\cos i - s_o L, & \Omega. \end{aligned} \tag{3}$$

The variables (a,e,i,M,ω,Ω) represent the classical elements defining the mean orbit associated with a given trajectory. Additionally, s_o is the integer nearest the ratio:

satellite mean motion over Earth rotation rate (i.e., $s_o = 2$ is associated with a 12 hr orbit), μ is the Earth's reduced mass, θ_e is the Greenwich sidereal angle and $\dot{\theta}_e$ is its associated rate. The quantity $\Omega_\mathcal{L}$ is the longitude of the ascending node of the lunar orbit (referenced to the ecliptic plane), and Ω_S is the ascending node of apparent solar orbit (referenced to the equatorial plane). Note that the angle λ, called the stroboscopic mean node, has a slow variation in time due to the commensurability between satellite mean motion and the Earth's rotation rate (that is, $(\dot{M}+\dot{\omega})/s_o + \dot{\Omega} \approx \dot{\theta}_e$). Furthermore, the perigee ω and the right ascension of the ascending node Ω vary slowly, primarily because of Earth's oblateness. The ascending nodes $\Omega_\mathcal{L}$ and Ω_S vary linearly with time.

STATIONKEEPING PERFORMANCE AS A FUNCTION OF ECCENTRICITY

A Poincaré section is a useful tool for analyzing the relationship between eccentricity and the chaotic regions of phase space produced by an eccentric, commensurate orbit. Figure 1 displays two plots, the upper one is a Poincaré section of orbits with initial values of (a,e,i,Ω,ω,M) = (various periods near 12 hrs, 55°, .01, 0°, 65°, -47°) ; the lower plot is similar except the initial eccentricity has been increased to .02. The dynamical model used to produce the trajectories is long period with secular oblateness effects and critical tesseral harmonics up to 4th order and degree (no other zonal and luni-solar perturbations are present). Note the existence of chaotic regions in both plots (identified by the scattered dots), and the marked increase in the complexity and extent of these regions in the plot with e = .02 as compared to e = .01. Prior research has shown that the implication of these complex dynamics is that the traditional east-west stationkeeping method is much more likely to become unstable (that is, the action rate $\dot{I}_1$ or, equivalently, the nodal acceleration $\ddot{\lambda}$ changes sign during a stationkeeping cycle) in these regimes.[2] To assess this possibility, it is instructive to analyze the equations of motion associated with a satellite that is controlling its stroboscopic mean node to remain within a specified deadband region (i.e., east-west SK),

$$\dot{I} = \sum_{q=0} m h^7_{lmpq}(a^*,e^*,i^*)\sin[m(\lambda-\lambda_{lm})] + \sum_{q\neq 0} m h^7_{lmpq}(a^*,e^*,i^*)\sin[m(\lambda-\lambda_{lm})-q\omega(t)], \quad (4a)$$

$$\dot{\lambda} = -\frac{3}{s_o^2 a^{*2}} I, \quad (4b)$$

$$\dot{\omega} \equiv \dot{\omega}_{\text{sec}} = \frac{\partial H_o}{\partial I_2^*} = \frac{3}{2}\frac{J_2 n^*}{\left(1-e^{*2}\right)^2}\left(\frac{R_e}{a^*}\right)^2\left(2-\frac{5}{2}\sin^2 i^*\right) \quad (4c)$$

Equation (4) represents a local dynamical model that is reduced from Equation (1), the reduction procedure can be found in reference [2]. It has 3/2-Degrees of Freedom (DOF) with phase variables that include the action $I \equiv I_1 - I_1^* = s_o(L-L^*) \approx$

Table 1: GPS Satellite Locations Nearest Action Rate Zeros

Sat ID	Ω (deg)	$u = \omega + M$ (deg)	λ (deg)
A4	188.089	58.638	14.698
E2	68.089	319.428	25.093
C2	308.089	28.628	119.693
B3	248.089	326.808	208.783

$s_o\sqrt{\mu/a^*}(a-a^*)/2$, the stroboscopic mean node λ, and perigee ω. The starred '*' parameters represent values of the associated variable at the location of the exact commensurability between the secular rates, that is $\dot{\lambda}=0$. Proceeding in a manner similar to the classical control strategy, the node in Eq. (4a) is fixed to a specified nominal value λ_n. It is around this nominal value that the stationkeeping process controls the orbit to remain inside of a specified deadband region $\Delta\lambda$. Within the deadband the node is allowed to drift. Stationkeeping maneuvers are performed when the orbit drifts to a boundary of the deadband. Utilization of this control strategy changes the nature of the dynamic response of the perturbing tesseral harmonics ($h^7_{lmpq}(\cdot)\sin(\cdot)$ in Eq (4a)). Because λ is nearly stationary, the terms with $q=0$ can be considered constant. However, the terms with $q\neq 0$ are nonautonomous because of their dependence on perigee (a time varying quantity). This functional dependence on time invalidates two fundamental assumptions in the classical stationkeeping method: the nodal time history is not symmetric around the exact resonance value, and the nodal acceleration is not guaranteed to have a constant sign within a cycle (or, equivalently, the action rate can pass through a value of zero).

To determine regions of phase space that have the potential to encounter a passage through an action rate zero set Eq. (4a) equal to zero. The result yields a function of node λ and perigee ω that is parameterized by eccentricity when the semi-major axis is set to the exact resonance value a^* and the inclination is specified. In the case of a GPS orbit, the resonant semi-major axis takes the value 26560 km (i.e., a 12 hr orbit), and the inclination is set to 55°. Figure 2 plots the location of the action rate zeros for selected values of eccentricity. Note that the behavior of these locations becomes increasingly complex with a modest growth in eccentricity. Now, at an inclination of 55°, perigee varies in a nearly secular fashion, and, for a mission lifetime of 10 years it can be expected to change by ~100°. Hence, if a satellite initial condition is placed near a line of zeros with an irregular shape, there exists an increased possibility of encountering the zero as perigee evolves. This possibility also becomes greater with an increase of initial eccentricity.

To investigate this two examples are considered using elements selected from the GPS constellation,[4] but with eccentricities that are modified slightly from the ideal circular case. Some of the mean elements that are common to all the satellites in the GPS constellation include semi-major axis and the inclination, which take the values defined

previously. The elements that are unique for each satellite in the constellation include the ascending node Ω and the argument of latitude ($u = \omega + M$). These elements are carefully selected so that the GPS constellation can achieve its required coverage objectives (i.e., 4 satellites inview at any ground station at all times). On the other hand, specifications for eccentricity and perigee are secondary. Optimally, eccentricity should be zero, and perigee would be undefined. However, this is an idealized situation that is never realized in practice. The actual orbits always posses some latent eccentricity, and, hence, a value for perigee. Indeed, the GPS program has a requirement to inject into the final drift orbit with an eccentricity no greater than .012.[4] Thus, it is entirely possible that a particular combination of elements could yield a situation where the node will encounter a zero. Table 1 lists those satellites in the planned GPS constellation[4] that have values of the stroboscopic mean node nearest the action rate zero locations, as shown in Figure 2. These orbits have the most potential to encounter SK instabilities in their lifetimes. Note the epoch associated with the elements is April 15, 1999, this yields a mean Earth sidereal angle of θ_e= 202.71°. The two cases studied are associated with satellite ID A4. In the first case the initial eccentricity has a value of .01, and in the second it is initially .02. In both cases perigee has been set to zero. The selected deadband region has a width of 4° and a nominal nodal value of $\lambda_n = 14.698°$. The boxes shown in Figure2 for e = .01, and .02 have sides with lengths equal to the deadband and a 100° change in perigee (i.e., a 10 yr mission). The boxes indicate the possibility of encountering an action rate zero during the lifetime of a mission. Examination of Figure 2 shows that the selected initial conditions are such that the 1st case, with e = .01, does not encounter a zero over the satellite lifetime, and the 2nd case, with e = .02, does.

Both cases utilize the Eccentric Orbit Stationkeeping (EOSK) algorithm developed in reference [2] for use with orbits that encounter action rate zeros. The controlled orbits are simulated for several thousands days with the results for semi-major axis, eccentricity, and node shown in Figures 3 and 4. The force model used in the propagation includes tesseral, zonal, lunar, and solar effects. In Figure 3, as expected, the trajectory does not encounter an action rate equal to zero, thus the nodal history exhibits the traditional 'scallop' shape. In the second case, the trajectory passes through an action rate equal to zero, as seen in Figure 4. Evidence of this can be seen in the irregular nodal histories during the second cycle from 1100 to 2400 days. This is typical of the EOSK algorithm as it changes its grazing and burn boundaries to accommodate the sign change in the nodal acceleration. The EOSK algorithm is successful at keeping the node within the desired deadband region during the entire mission. It is important to note that, for this set of initial conditions, the traditional east-west stationkeeping algorithm would have become unstable during the 2nd cycle, and would *not* have been able to maintain the node within the desired deadband region. The other point of note is the behavior of eccentricity, in the first case there was a variation of approximately Δe ~.003 and in the second the variation was ~ .004. Clearly, a different value for initial perigee or epoch coupled with a shift in eccentricity could bring the orbit into a regime where an action rate zero can occur during the mission lifetime. A better understanding of the behavior of eccentricity is desirable so that the SK instability issue can be more thoroughly assessed.

LONG TERM ECCENTRICITY BEHAVIOR

The previous discussion illustrated the central role that eccentricity has in determining the possibility of an encounter with an action rate zero. Thus, it would be beneficial to develop an analytical representation for the behavior of eccentricity as a function of time. Much has been published in this area, and it is conventional wisdom that luni-solar perturbations can have a significant impact on the behavior of eccentricity. Giacaglia[5] has written a thorough review of nearly 40 years of published results regarding the effects of luni-solar perturbations on artificial satellite orbits. However, most prior work has not dealt with the issue of lunar resonance overlap and its consequences on long-term eccentricity behavior. Ely and Howell[3] have shown that there exists an intricate web of luni-solar resonances that can interact to produce chaotic and diffusive motion. The locations of the significant resonances can be located by analyzing linear combinations of the form $m_1\dot{\omega}+m_2\dot{\Omega}+m_3\dot{\Omega}_{\mathcal{L}}\approx 0$ or $m_1\dot{\omega}+m_2(\dot{\Omega}-\dot{\Omega}_{\mathcal{S}})\approx 0$, where (m_1,m_2,m_3) represent a vector of numbers. The resonance interactions have dominant effects on the extremely long term behaviors of $\{e,i,\omega,\Omega\}$. Eventhough the time scale for such motions are typically much longer than that of a satellite mission, it is instructive to understand the nature of the global dynamics and the time scales necessary to observe these dynamics. With this information it is possible to assess the time scales that an asymptotic theory will be valid. That is a first order averaging approach yields a solution that is accurate to $O(\varepsilon)$ on time scales of order $O(1/\varepsilon)$. An analysis of the potential for chaos and/or diffusion allows for a more quantitative assessment of this time scale.

To illustrate the phenomena a selected GPS-like initial condition, (a,e,i,ω,Ω,M) = (26560 km, .02., 55°, 0°, 8°, 52°), is propagated for approximately 60,000 years. The dynamical model used consists of only long period luni-solar perturbations (geopotential terms other than secular oblateness are not present). This yields a set of dynamical equations that are not stiff, hence amenable to such a long term propagation. To illustrate the behavior of the motion, the inclination and eccentricity are sampled on returns to a specified ascending node value (arbitrarily selected to be 100°), and plotted as a point on the inclination/eccentricity plane. The time span between consecutive points is approximately 20 years. The results are shown in Figure 5 as an array of plots. Each plot is a snap shot in time. The upper left plot represents the first 500 samples (~ 9950 years), and the lower left includes all 3000 samples (~ 59,692 years). Also shown on the plots are the locations of the significant luni-solar resonances (i.e., $m_1\dot{\omega}+m_2\dot{\Omega}+m_3\dot{\Omega}_{\mathcal{L}}\approx 0$ or $m_1\dot{\omega}+m_2(\dot{\Omega}-\dot{\Omega}_{\mathcal{S}})\approx 0$) as functions of inclination and eccentricity. They appear as the complex web of intersecting lines. The initial condition is indicated on the diagram and is located near the dominant luni-solar resonances that impact the GPS constellation. Specifically, the largest nearby resonance is associated with luni-solar harmonic terms that have an angular argument of $(2\omega+\Omega)$. The straight line at the 56° inclination (at all eccentricities) identifies the resonance location. The other resonance is associated with a lunar harmonic with angular argument of $(2\omega+\Omega_{\mathcal{L}}-\pi)$. This produces the curved line beginning at approximately 53.3°. Clearly, for the first 1000 points the trajectory remains

confined to the region of these two resonances. The behavior is actually chaotic, however the motion does not exhibit any large scale excursions in eccentricity or inclination. Then between 1000 and 1500 samples the trajectory experiences large scale diffusion. As is typical of this type of motion, there exists a tendency for the trajectory to follow a resonance curve, and then, at an intersection with another resonance, it jumps to follow the other curve. The example also illustrates the potential for an initially near circular orbit to become nearly hyperbolic under the influence of only luni-solar perturbations.

ANALYTICAL ECCENTRICITY MODEL

Since mission time scales, which are on order of 10 – 15 years, are much shorter than the time frames illustrated in Figure 5 it is reasonable to expect an asymptotic theory to produce qualitatively accurate eccentricity histories for the span being considered. Indeed, results will show that the analytical model developed in this study compares favorably with numerically generated results. Specifically, the behavior of eccentricity in the region of a GPS orbit is of interest; therefore the model includes only those perturbations that dominate near an inclination of 55° and with eccentricities near zero. The harmonic terms are analyzed by the magnitude of their coefficients divided by the secular rate of their angular argument (i.e., the magnitude of the harmonic coefficients of the analytically integrated solution). Those with the largest coefficients are retained. Also, note that, for the time scale of interest, the orbit is only in shallow resonance with harmonic terms of the form $h(a,e,i)\cos(2\omega+\Omega)$. It is sufficiently shallow that a standard perturbation method can be utilized to integrate the equation of motion that includes this term. The other resonance terms have insufficient time to impact the motion significantly, and can be neglected. As the previous discussion indicated, if the time scale were longer these assumptions would not be valid.

The other key feature affecting the behavior of eccentricity is associated with the tesseral harmonics. Controlling the stroboscopic node to be nearly stationary introduces a coupling between eccentricity and the tesseral harmonics that would not ordinarily exist because the time scale of the nodal advance is much faster than that of perigee. However, since the controlled nodal rate is effectively zero, the angular rate associated with the some of the tesseral harmonics can now be attributed primarily to the perigee rate. With the preceding observations in mind, a Hamiltonian of long period terms can be formulated that is specialized for the phase space region applicable to the class of orbits that are near circular and at an inclination near 55°. It is written formally as,

$$
\begin{aligned}
H_{\mathrm{GPS}} &= V_{\mathrm{GPS}}^{SEC} + V_{\mathrm{GPS}}^{2} + V_{\mathrm{GPS}}^{5} + V_{\mathrm{GPS}}^{7} + V_{\mathrm{GPS}}^{3}, \\
&= \begin{cases} V_{\mathrm{GPS}}^{SEC} + \\ (h_{2\omega}^{2} + h_{2\omega}^{5})\cos 2\omega + h_{2\omega+\Omega}^{2}\cos 2\omega+\Omega + h_{2\omega+\Omega-\Omega_{\varsigma}}^{5}\cos 2\omega+\Omega-\Omega_{\varsigma} + \\ h_{2(\lambda-\lambda_{32})}^{7}\cos 2(\lambda-\lambda_{32}) + h_{2(\lambda-\lambda_{22})+\omega}^{7}\cos 2(\lambda-\lambda_{22})+\omega + \\ h_{2(\lambda-\lambda_{22})-\omega}^{7}\cos 2(\lambda-\lambda_{22})-\omega + h_{\pi/2-\omega}^{3}\cos(\pi/2-\omega) \end{cases}
\end{aligned}
\qquad (5)
$$

where the secular term includes Earth's oblateness and luni-solar contributions. This term yields the secular rates for perigee $\dot{\omega}_{\text{sec}}$ and the ascending node $\dot{\Omega}_{\text{sec}}$. The detailed equations for these rates and the long-period harmonic terms in Eq. (5) are found in the appendix. Note, that the lunar orbital parameters are referenced to the ecliptic plane, and all others (including the solar parameters) are referenced to the Earth's equatorial plane. For purposes of the analytical model, the node λ and solar ascending node Ω_s are held constant. The equation of motion for eccentricity is obtained by applying following perturbation equation to Eq. (5),

$$\frac{de}{dt} = \frac{\sqrt{1-e^2}\,(1-\sqrt{1-e^2})}{s_o n a^2 e}\frac{\partial H}{\partial \lambda} + \frac{\sqrt{1-e^2}}{na^2 e}\frac{\partial H}{\partial \omega} \approx \frac{e}{2 s_o n a^2}\frac{\partial H}{\partial \lambda} + \frac{1}{na^2 e}\frac{\partial H}{\partial \omega}. \tag{6}$$

Proceeding in the standard way, the equation of motion can be analytically integrated by holding the harmonic coefficients constant and using the secular rates to evaluate the angles as linear functions of time. The result is an equation for eccentricity that is a function of time and the initial mean elements, and, formally, takes the form,

$$e(t) = e_o + \sum_{\{(m_1,m_2,m_3,m_4,m_5)\}} \frac{C(a_o, e_o, i_o; \text{parameters})}{m_1\dot{\omega} + m_2\dot{\Omega}} \left\{ \begin{array}{l} \cos\left(m_1\omega(t) + m_2\Omega(t) + m_3\lambda_n + m_4\Omega_s + m_5\frac{\pi}{2}\right) - \\ \cos\left(m_1\omega_o + m_2\Omega_o + m_3\lambda_n + m_4\Omega_s + m_5\frac{\pi}{2}\right) \end{array} \right\}, \tag{7}$$

where the set of vectors $\{(m_1, m_2, m_3, m_4, m_5)\}$ specifies the linear combinations of angles found in Eq. (5). The coefficients $C(a_o, e_o, i_o; \text{parameters})$ are functions of the initial mean elements and parameters such as, the harmonic coefficients J_{lm} and the third body orbit elements.

The analytical model defined in Eq. (7) yields a convenient method for ascertaining the behavior of eccentricity over time as a function of initial values. As an illustrative example consider a satellite with $(\Omega, \lambda_n) = (188.089°, 19.638°)$, this represents Sat A4 with a slightly different argument of latitude (u = 64.638°) or a slightly different defining epoch time ($\theta_e = 197.71°$). The initial eccentricity has been set at e = .01. Using these values, eccentricity is computed as function of the initial perigee value and time and illustrated in Figure 8. It is evident from the figure that most values of perigee below 180° yield eccentricities that grow to near .015, and above 180° many approach zero. Note there is a small region where the eccentricity is less than zero, this is an artifact of the perturbation method. A potential technique to avoid this is to rescale Eq. (6) by dividing by e and integrating as before. Doing so yields a function of time for eccentricity that formally has the form,

$$e(t) = e_o Exp\left[\sum \frac{C}{e_o(m_1\dot{\omega} + m_2\dot{\Omega})}\cos(\cdot)\right]. \tag{8}$$

This approach was initially utilized for this study, with good results. Indeed, using the same conditions as those utilized to make Figure 6 and applied to Eq. (8) produce the eccentricity behavior illustrated in Figure 7. Now there is no region that yields negative values for eccentricity and qualitatively the results are very similar to those from the standard theory. However, unlike the standard approach, the result in Eq. (8) has terms of order $O(J_{22}/e_o)$ because of the coupling with the tesseral harmonics. This result is not asymptotic as $e_o \to 0$, hence the predicted behavior diverges from the true behavior. Numerically, if the coupling tesseral terms yield an order of less than $O(1)$, then Eq. (8) yields satisfactory results as seen in Figure 7. However this result is local and nonuniform in e_o. Since Eq. (7) is uniform, it is preferred for assessing the qualitative behavior of eccentricity.

Returning to the example of Sat A4 with the modified nominal node ($\lambda_n = 19.638°$), the shift in node coupled with an anticipated growth of eccentricity of $\Delta e = .003$ places the satellite trajectory in a region that should encounter an action rate zero (see Figure 2). The controlled trajectory result is shown in Figure 8. It is evident from the semi-major axis history and the nodal history that the trajectory passes through an action rate zero during the third cycle (1900 to 3500 days). The EOSK algorithm compensates by redefining target boundaries and performing a maneuver to drift to the new burn boundary (~ 18°). The behavior of eccentricity is shown in the middle plot. The numerically propagated result is shown with the solid line and the analytically propagated result (using Eq. (7)) is shown with the dashed line. The analytical result correctly captures the qualitative behavior, and is quantitatively accurate to within 10% of the true values. Comparisons (not shown) with the other trajectories examined in this study yield similar qualitative and quantitative agreement. Using the combination of the action zero locations predicted using Eq. (4a) and the analytical behavior of eccentricity from Eq. (7), it is now possible to ascertain the likelihood that a specific GPS mission will encounter an action rate zero and need to utilize a robust SK approach, such as the EOSK algorithm.

CONCLUSION

These results indicate that an orbit inclined at 55° with modest eccentricity can encounter significant regions of phase space that have action rate zeros. The location of these zeros is primarily a function of the nominal stroboscopic node, perigee, and eccentricity. As seen in Figure 2, the curves defining these locations become increasingly complex with a modest growth in eccentricity. This study has also shown that the combined interaction of luni-solar perturbations and tesseral harmonics (with a stationary stroboscopic node) dominates the behavior of eccentricity, and can lead to a growth of eccentricity. Indeed, it is possible that eccentricity changes over a mission lifetime can put a satellite orbit that, initially avoided action rate zeros, into a region of space where it

will likely encounter them. This has potentially significant operational impacts. The next phase GPS satellites are to be delivered into their final orbits with eccentricities not to exceed 0.012.[4] The preceding analysis shows that GPS satellites in orbits with borderline eccentricities may run the risk of encountering SK instabilities using traditional techniques. Utilization of an enhanced SK method (such as the EOSK approach), repositioning the satellite to avoid the action rate zeros, or controlling eccentricity are all potential solutions to this problem. At a minimum, once an operational orbit is attained an assessment should be made as to likelihood of the satellite encountering these instabilities during the mission lifetime.

ACKNOWLEDGEMENTS

This research was partially supported by the Jet Propulsion Laboratory, California Institute of Technology, under contract with the National Aeronautics and Space Administration. The author would like to thank John Cox, George Chao, James Gidney, and Matthew Hart of The Aerospace Corporation for their helpful discussions regarding this work, and for providing details regarding the GPS constellation operational requirements and orbit parameters.

APPENDIX

Detailed equations for the secular rates are as follows,

$$\begin{aligned}\dot{\omega}_{\text{sec}} = &\frac{3}{4}\frac{nJ_2}{(1-e^2)^2}\left(4-5\sin^2 i\right)+\\ &\frac{3}{512}\frac{n_{\leftmoon}^2}{n}\frac{\left[8+7e^2+(16+9e^2)\cos 2i\right]}{(1-e^2)^2}\left(1+3\cos 2i_{\leftmoon}\right)\left(1+3\cos 2o_e\right)+\\ &\frac{3}{128}\frac{n_{\odot}^2}{n}\frac{\left[8+7e^2+(16+9e^2)\cos 2i\right]}{(1-e^2)^2}\left(1+3\cos 2i_{\odot}\right)\ ,\end{aligned} \tag{9}$$

$$\begin{aligned}\dot{\Omega}_{\text{sec}} = &-\frac{3}{2}\frac{nJ_2}{(1-e^2)^2}\cos i-\\ &\frac{3}{128}\frac{n_{\leftmoon}^2}{n}\frac{(2+3e^2)\cos i}{(1-e^2)^2}\left(1+3\cos 2i_{\leftmoon}\right)\left(1+3\cos 2o_e\right)-\\ &\frac{3}{32}\frac{n_{\odot}^2}{n}\frac{(2+3e^2)\cos i}{(1-e^2)^2}\left(1+3\cos 2i_{\odot}\right)\ ,\end{aligned} \tag{10}$$

where n, $n_{\leftmoon}$, and $n_{\odot}$ refer to the mean motion rates of the satellite, the Moon, and the Sun, respectively. The angle o_e is the obliquity of the ecliptic. Recall that all lunar orbit parameters are referenced to the ecliptic plane, and solar apparent orbit parameters are referenced to the Earth's equatorial plane. Detailed equations for the long period harmonic terms identified in the Hamiltonian of Eq. (5) take the form,

$$V_{\mathrm{GPS}}^{4} = e^2 \frac{\mu_4}{a_4}\left(\frac{a}{a_4}\right)^2\left(\frac{3}{4}\sin^2 i_4 - \frac{1}{2}\right)\left\{\begin{array}{l}\frac{15}{8}\sin^2 i(1+3\cos o_\varepsilon)\cos 2\omega - \\ \frac{15}{16}\sin i(1+\cos i)\sin 2o_\varepsilon \cos 2\omega + \Omega\end{array}\right\} + O(e^3), \qquad (11)$$

$$V_{\mathrm{GPS}}^{5} = e^2 \frac{\mu_5}{a_5}\left(\frac{a}{a_5}\right)^2\left\{\begin{array}{l}\frac{15}{8}\sin^2 i\left(\frac{3}{4}\sin^2 i_5 - \frac{1}{2}\right)\cos 2\omega + \\ \frac{15}{16}\sin i(1+\cos i)\sin i_5 \cos i_5 \cos 2\omega + \Omega - \Omega_5\end{array}\right\} + O(e^3), \qquad (12)$$

$$V_{\mathrm{GPS}}^{7} = -\frac{\mu}{a}\left\{\begin{array}{l}\frac{15}{8}\left(\frac{R_e}{a}\right)^3 \sin i(1-2\cos i - 3\cos^2 i)J_{32}\cos[2(\lambda-\lambda_{32})] - \\ \frac{3}{8}e\left(\frac{R_e}{a}\right)^2 (1+\cos i)^2 J_{22}\cos[2(\lambda-\lambda_{22})+\omega] + \\ \frac{9}{4}e\left(\frac{R_e}{a}\right)^2 \sin^2 J_{22}\cos[2(\lambda-\lambda_{22})-\omega]\end{array}\right\} + O(e^2). \qquad (13)$$

$$V_{\mathrm{GPS}}^{3} = -\frac{3}{2}e\frac{\mu}{a}\left(\frac{R_e}{a}\right)^3 J_3\left\{\frac{5}{4}\sin^3 i - \sin i\right\}\cos\frac{\pi}{2} - \omega + O(e^3). \qquad (14)$$

REFERENCES

1. Ely, T. A., and Howell, K. C. "Long Term Evolution of Artificial Satellite Orbits Due to Resonant Tesseral Harmonics," *Journal of the Astronautical Sciences*, Vol. 44, No. 2, April - June 1996.
2. Ely, T. A., and Howell, K. C. "East-West Stationkeeping of Satellite Orbits with Resonant Tesseral Harmonics." *ACTA Astronautica* (accepted for publication).
3. Ely, T. A., and Howell, K. C. "Dynamics of Artificial Satellite Orbits with Tesseral Resonances Including the Effects of Luni-Solar Perturbations." *International Journal of Dynamics and Stability of Systems*, Vol. 12, No. 4, December 1997.
4. Gidney, J., Astrodynamics Department, The Aerospace Corporation, private communication, May 1999.
5. Giacaglia, G. E. O., "Third Body Perturbations on Satellites." *Proceedings of the Artificial Satellite Theory Workshop*, U.S. Naval Observatory, Nov 8-9, 1993.

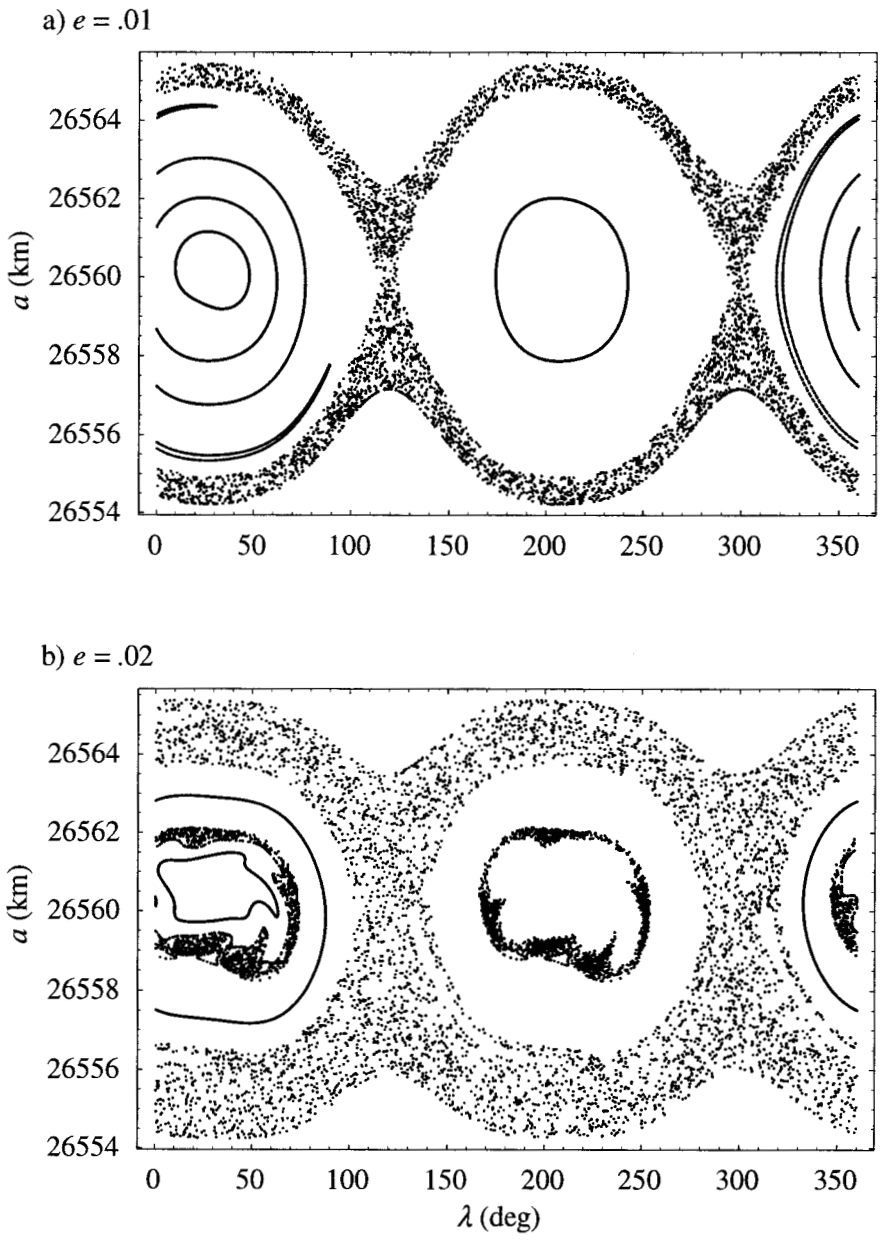

Figure 1: Poincaré section of GPS class of orbits for different eccentricities ($\omega = 65°$)

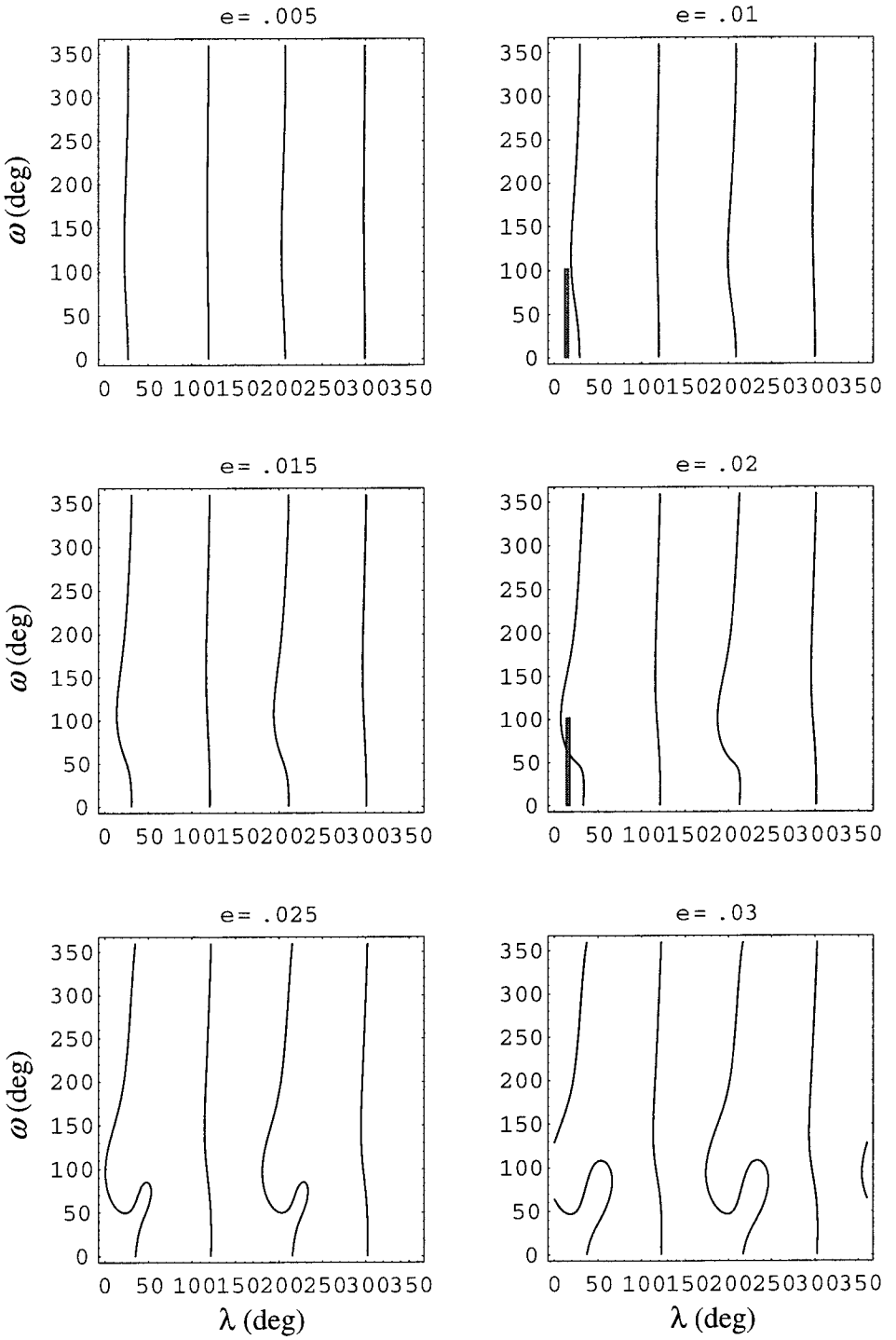

Figure 2: Action rate zeros parameterized by eccentricity

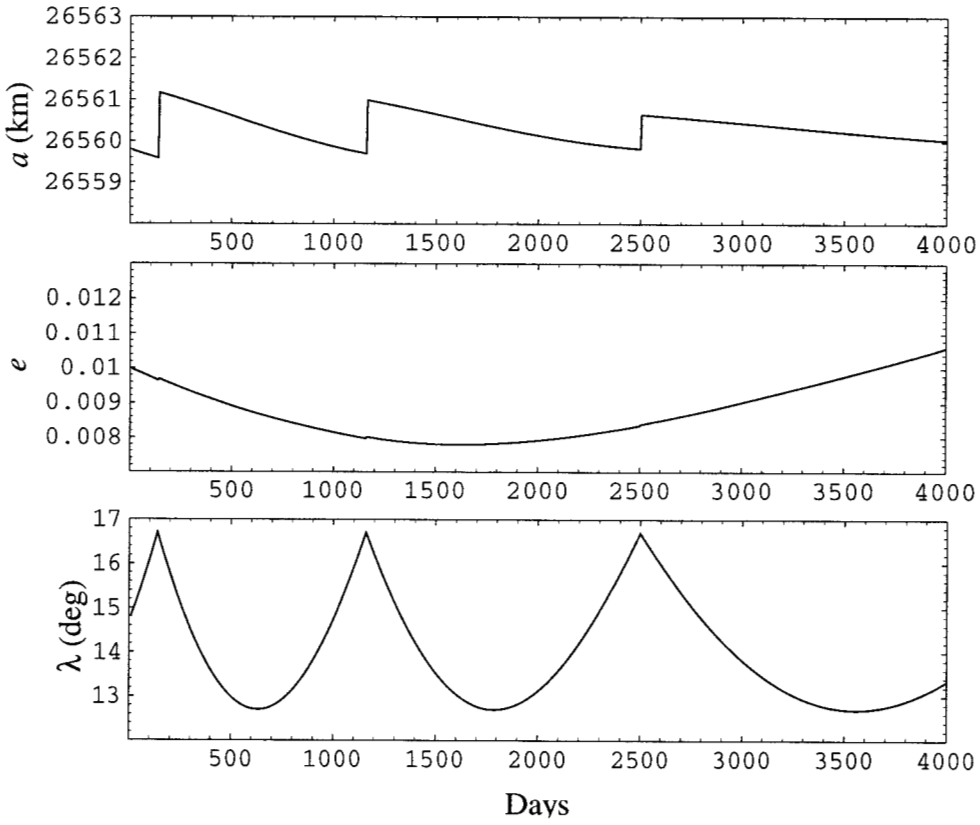

Figure 3: Stationkeeping cycle for the case with e = .01. No action rate zeros encountered.

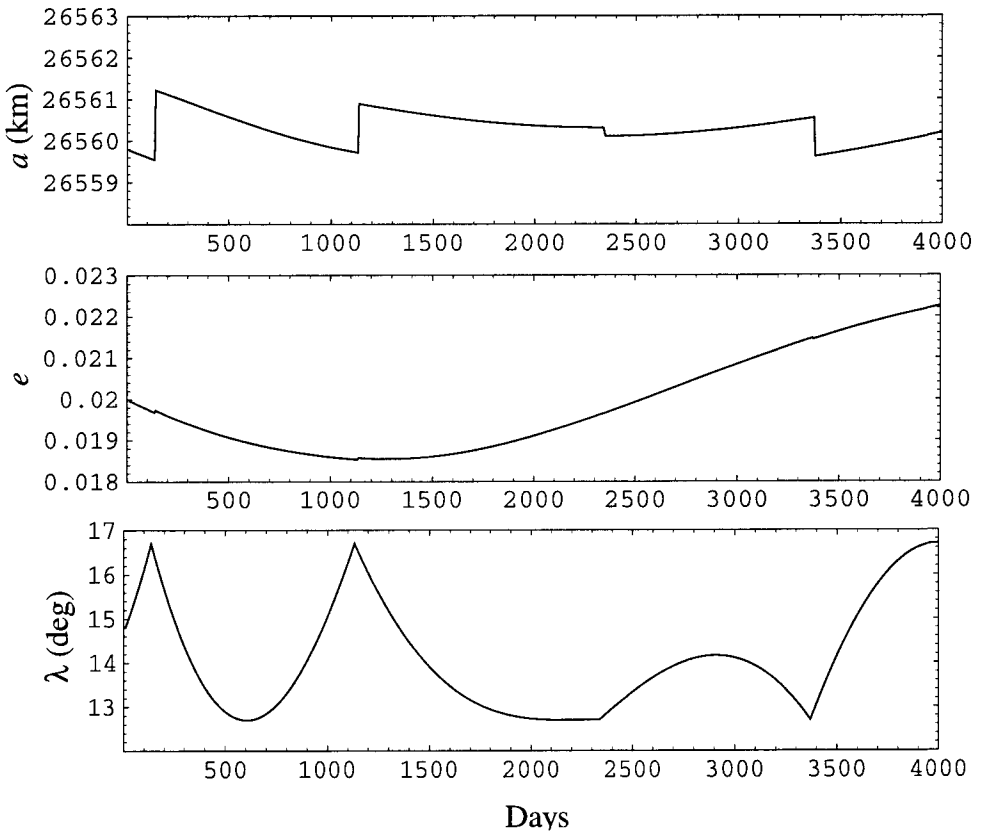

Figure 4: Stationkeeping cycle for the case with e = .02. Action rate zero encountered in the third cycle (1100 to 2400 days) and the EOSK algorithm compensates for zero.

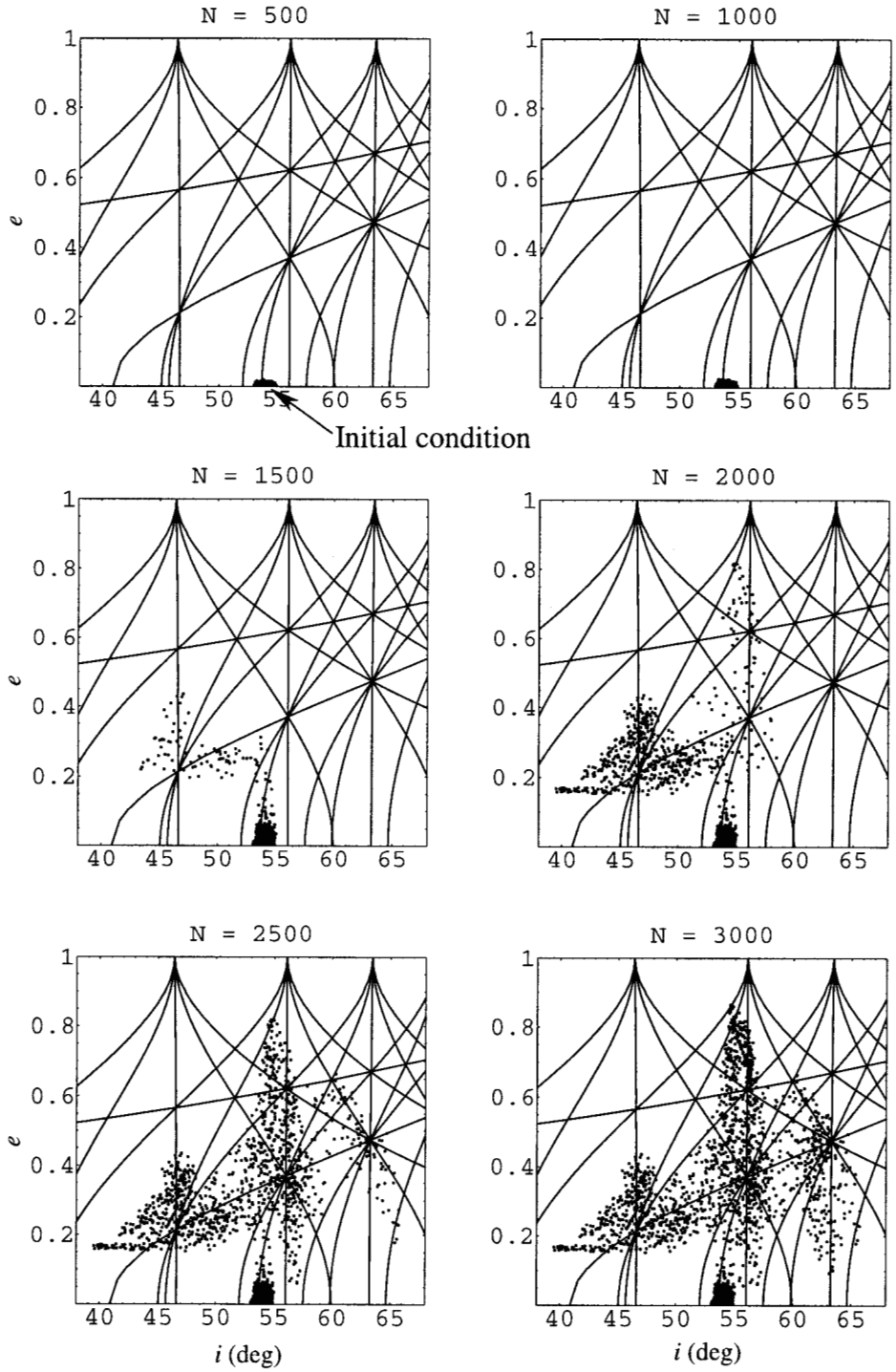

Figure 5: Extremely long term behavior of eccentricity vs. inclination for a GPS like orbit. The dynamics illustrate chaos and diffusion as it follows resonance locations.

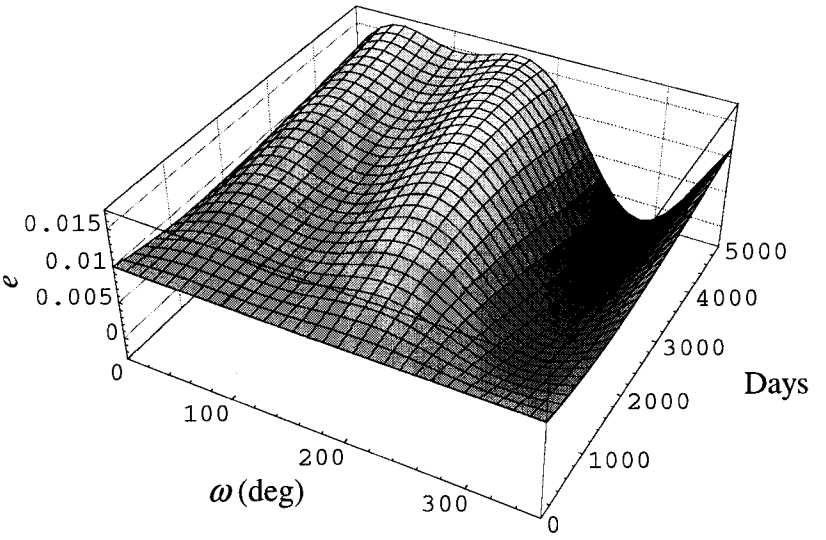

Figure 6: Analytical eccentricity behavior as a function of initial perigee and time, obtained using standard perturbation theory.

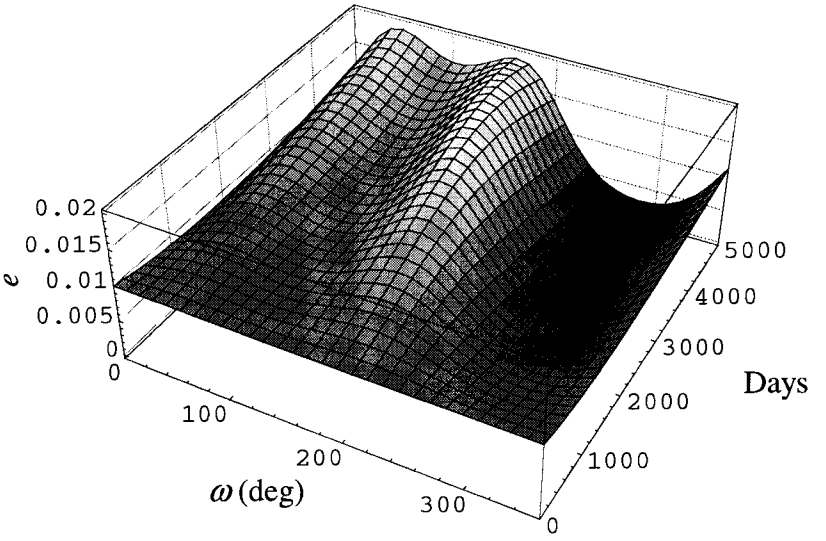

Figure 7: Analytical eccentricity behavior as a function of initial perigee and time, obtained using standard perturbation theory.

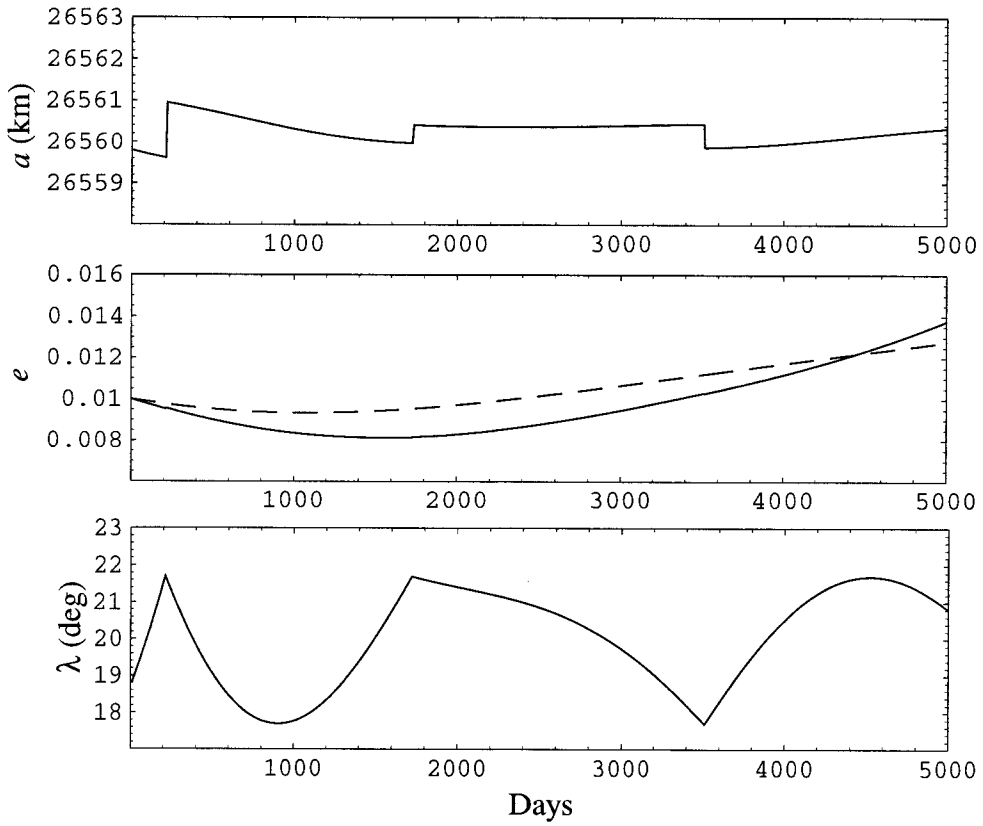

Figure 8: Same initial conditions as in Figure 3 except perigee has been shifted from an initial value of 0° to 8°. An action rate zero is encountered and the EOSK algorithm compensates. Note that the dashed line in the eccentricity figure represents the analytically predicted value using the standard perturbation theory, Eq. (7).